Energy and Exergy Analysis for Mixed Convection in a Microstructure Filled Vented Cavity: Effect of Change of Aspect Ratio

M. H. Banna*, S. F. Barna* and A. K. M. S. Islam*

ABSTRACT

In this study, an enclosure filled with fluid saturated porous medium is considered. Initial observations are taken with all walls being isothermal. Imposing adiabatic conditions on three walls and isothermal condition on left vertical wall, a second stage of observations are carried out. Natural convection takes place due to the temperature difference between the isothermal wall and the fluid. Forced convection is induced by providing an inlet at the bottom surface and a vent at the top, facing the inlet. The problem is solved using the modified Darcy flow model and energy equation for five different Rayleigh Numbers (1, 50, 100, 500, and 1000) and seven different Peclet Numbers (0.1, 1, 5, 10, 20, 50 and 100). The equations are solved using standard Finite Element Method for considering three different Aspect Ratios of the cavity.

Keywords: *Mixed Convection, Porous Media, Aspect Ratio, Vented Cavity.*

1 INTRODUCTION

Heat transfer by mixed convection in saturated porous media has attracted worldwide attention owing to its fundamental importance & wide range of applications. The overgrowing requirement for energy, the necessity to develop effective technologies for nuclear waste management, transpiration cooling, separation processes in chemical industries, building thermal insulations, winding structure for high-power density in electric machines, packed-bed catalytic reactors and numerous other applications have led to a considerable

*Department of Mechanical and Chemical Engineering, IUT, Bangladesh
Email: banna9118117@yahoo.com

interest in convective heat transport through porous media. The same processes are also found naturally within living organisms, such as in biological membranes and filters and the flow of blood or other body fluids. The pores in the media traps fluid which can easily be subjected to vaporization, condensation or to migration as a result of applied pressure gradient.

A rich variety of important analytical, numerical, and experimental results have been demonstrated in the books by Nield and Bejan [1], Ingham and Pop [2–4], Vafai [5,6], Pop and Ingham [7], Bejan and Kraus [8], Ingham et al. [9] and Bejan et al. [10], and the review articles by Hadim and Vafai [11], and Vafai and Hadim [12] The technical issues of mixed convection flow in porous media have been concerned mainly with situations in which buoyancy effects are substantial, if not entirely dominant. So the flow regime of interest is clearly the flow situations where buoyancy effects are substantial or dominant.

Henry Darcy's experimental studies in 1856 of saturated water flow through a homogeneous porous medium contained in a vertical column have provided the basis for the quantitative description of fluid flow in a wide variety of both natural and engineered porous medium environmental systems. Oddmund and Tyvand [13] in 1979 investigated theoretically convection currents in an isotropic porous media. The supercritical steady two-dimensional motion, the heat transport and the stability of the motion are investigated. Some of the results may be applied in insulation techniques. K. Vafai [14] analysed the effects of variable porosity and inertial forces on convective flow and heat transfer in porous media. Specific attention was given to forced convection in packed beds in the vicinity of an impermeable boundary. After establishing the governing equations, a thorough investigation of the channeling effect and its influence on flow and heat transfer through variable-porosity media was presented. A. Younes [15] in 2004 developed an accurate finite-volume Eulerian Lagrangian localized adjoint method (ELLAM) for solving the one-dimensional variable coefficients advection dispersion equation that governs transport of solute in porous medium. The method uses a moving grid to define the solution and test functions. Numerical results for a constant-coefficient problem and a variable-coefficient problem are very close to analytical and fine-grid solutions, respectively. The porous layer is homogeneous and bounded by two infinite perfectly heat-conducting horizontal planes. The criterion for the onset of convection is derived. The supercritical steady two-dimensional motion, the heat transport and the stability of the motion are investigated. J. C.-F. & Wong, P. Yuan [16] showed that the consistent splitting scheme involving a mixed finite element method for considering the influence of the Forchheimer-extended Brinkman-Darcy model in the momentum equation is applied to double-diffusive convection in a fluid-

saturated porous medium. It is shown that the method is robust and can accurately predict flow, pressure distribution, and temperature and concentration fields. The numerical scheme may be an alternative to some other existing methods for the solution of porous thermosolutal convection problems since its implementation is very handy. Mahmud and Pop [17] in 2006 studied the mixed convection in a square vented enclosure filled with a porous medium. They determined the heat transfer characteristics varying the Rayleigh number, Peclet number, and the width of the inlet as a fraction of the height of the square enclosure over long ranges.

In this paper our attention has been focused on a problem of mixed convection. By providing an inlet and a square vent, forced convection condition can be imposed inside an enclosure filled with porous medium. Two different boundary conditions are imposed .Initially all the walls of the enclosure are at constant temperature. Subsequently it is followed by another analysis keeping only the left wall isothermal. The rest of the walls are adiabatic. The interaction between the buoyancy stemming from one or more heated elements inside the enclosure and the imposed forced flow forms the topic of our investigation.

In this numerical analysis, different aspect ratios of enclosure, different inlet outlet ratios, different inlet width to cavity width ratios, boundary conditions are considered. The performance of the enclosure is determined by flow visualization and by analyzing different parameters such as Bejan Number, Nusselt Number and Entropy Generation Number. The results will help to find out most effective Aspect Ratio.

2 BASIC EQUATIONS

At first, fluid flow are considered to take place through an enclosure where all of its walls are isothermal at a temp T_w (Fig.1 (a)). Afterwards analyses are also conducted for fluid flow through an enclosure with only left wall being isothermal while remaining walls are kept adiabatic (Fig.1 (b)). There is an inlet at the left corner of the bottom wall and the vent is on the left corner of the top wall. The widths of the inlet and vent are I and O respectively as shown in Fig. 1, and in this study we have considered $I/O = 0.5$. Buoyancy effects are induced due to the difference in temperature between the left vertical wall, T_w, and the through-stream temperature, T_0, which has a constant velocity, V_0, at the inlet of the enclosure. The inlet forced flow is fixed at the inlet and the temperature difference (T_w - T_0) considered here is positive which means it is an aiding flow.

The assumptions made for porous media to prepare mathematical model are: the fluid and the porous medium are in local thermal equilibrium; the properties of the fluid and the porous media are constant; the viscous drag and inertia terms

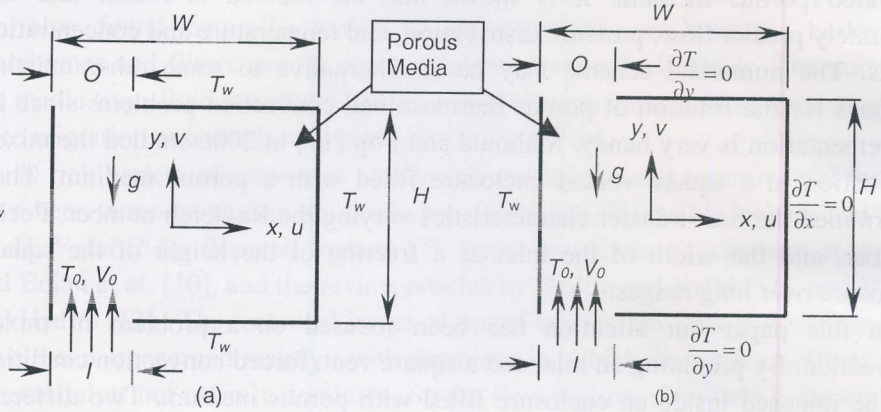

Figure 1: Physical model and the coordinate system of the cavity filled with porous media

of the momentum equations are negligible, and the Darcy and Boussinesq approximations are valid. Under these assumptions, the conservation equation for mass becomes:

$$\frac{\partial u}{\partial x}+\frac{\partial v}{\partial y}=0 \quad \ldots \quad \ldots \quad \ldots \quad \ldots \quad \ldots \quad (1)$$

The momentum flow inside the enclosure can be modeled by the Darcy flow model [1], by using the assumptions. This constructs a relationship between the flow velocities at a certain direction to the pressure gradient in that direction in vector form is,

$$\boldsymbol{v}=\frac{K}{\mu}(-\mathbf{grad}\, p+\rho\, \mathbf{g}) \quad \ldots \quad \ldots \quad \ldots \quad \ldots \quad \ldots \quad (2)$$

where $\boldsymbol{v}, K, \mu, p$, and $\mathbf{g}$ are the velocity vector, permeability, viscosity, pressure, and gravity vector, respectively. The permeability K is an empirical constant which may define a length scale squared of pores. Darcy's law becomes invalid in this kind of situation because it neglects the effects of solid boundary or the effects of a solid boundary or the inertial forces of the fluid flow. These effects are expected to be significant where the porosity of the medium is high. Again the Darcy flow model is applicable where the order of magnitude of the local pore Reynolds number, based on the local volume averaged speed $(|\boldsymbol{v}|^{1/2})$ and $K^{1/2}$ is smaller than 1. Taking **curl** on the both side of Eq. (2) with the assumption,

$$\boldsymbol{v} = u\boldsymbol{i} + v\boldsymbol{j} + 0\boldsymbol{k} \text{ and } \boldsymbol{g} = 0\boldsymbol{i} + g_y\boldsymbol{j} + 0\boldsymbol{k},$$

we can get

$$\frac{\partial u}{\partial y} - \frac{\partial v}{\partial x} = -\frac{g\beta K}{\nu}\frac{\partial T}{\partial x} \quad \ldots \quad \ldots \quad \ldots \quad \ldots \quad (3)$$

where $g = g_y$. Eq. (3) has no pressure term. Finally, the energy equation, according to Nield and Bejan [1], is

$$\sigma\frac{\partial T}{\partial t} + u\frac{\partial T}{\partial x} + v\frac{\partial T}{\partial y} = \alpha_m\left(\frac{\partial^2 T}{\partial x^2} + \frac{\partial^2 T}{\partial y^2}\right) \quad \ldots \quad \ldots \quad \ldots \quad (4)$$

Without any external or internal source, the equation of entropy generation according to Mahmud, S. and Fraser [18] is

$$S'''_{gen} = HTI + FFI = \frac{k}{T_0^2}\left[\left(\frac{\partial T}{\partial x}\right)^2 + \left(\frac{\partial T}{\partial y}\right)^2\right] + \frac{\mu}{KT_0}\left(u^2 + v^2\right) \quad \ldots \quad (5)$$

where, $$HTI = \frac{k}{T_0^2}\left[\left(\frac{\partial T}{\partial x}\right)^2 + \left(\frac{\partial T}{\partial y}\right)^2\right] \quad \ldots \quad \ldots \quad \ldots \quad \ldots \quad \ldots \quad (6)$$

and $$FFI = \frac{\mu}{T_0 K}\left(u^2 + v^2\right) \quad \ldots \quad \ldots \quad \ldots \quad \ldots \quad \ldots \quad \ldots \quad \ldots \quad (7)$$

Finally, the equation of energy flux density vector according to Mahmud S. and Fraser [18] is

$$\mathbf{E} = E_x\mathbf{i} + E_y\mathbf{j} = \rho\mathbf{v}\left[\frac{1}{2}|v|^2 + C_P(T\text{-}T_0)\right] - k\,\mathbf{grad}(T) \quad \ldots \quad \ldots \quad \ldots \quad (8)$$

where x, y are the Cartesian coordinates measured in the horizontal and vertical directions, u, v are the velocity components along x- and y-axes, and T is the fluid temperature, respectively,

We define the stream function ψ, in the usual way as

$$u = \frac{\partial \psi}{\partial y} \quad \ldots \quad \ldots \quad \ldots \quad \ldots \quad \ldots \quad \ldots \quad \ldots \quad (9)$$

$$v = -\frac{\partial \psi}{\partial x} \quad \ldots \quad \ldots \quad \ldots \quad \ldots \quad \ldots \quad \ldots \quad \ldots \quad (10)$$

Substituting Eqs. (9) and (10) into Eqs. (3) and (4), the following equations are obtained:

$$\frac{\partial^2\psi}{\partial x^2}+\frac{\partial^2\psi}{\partial y^2}=-\frac{g\beta k}{\nu}\frac{\partial T}{\partial x} \quad \ldots \quad \ldots \quad \ldots \quad \ldots \quad \ldots \quad (11)$$

$$\frac{\partial T}{\partial t}+\frac{\partial\psi}{\partial y}\frac{\partial T}{\partial x}+\frac{\partial\psi}{\partial x}\frac{\partial T}{\partial y}=\alpha_m\left(\frac{\partial^2 T}{\partial x^2}+\frac{\partial^2 T}{\partial x^2}\right) \quad \ldots \quad \ldots \quad \ldots \quad (12)$$

where *Ra* and *Pe* are the Rayleigh and Pe´clet numbers for a porous medium which are defined by

$$Ra=\frac{gK\beta(T_w-T_0)H}{\alpha_m\nu}, \qquad Pe=\frac{V_0 H}{\alpha_m} \quad \ldots \quad \ldots \quad \ldots \quad (13)$$

It is worth mentioning that the Rayleigh number may be either positive, $T_w > T_0$ (aiding flow) or negative, $T_w < T_0$ (opposing flow), respectively. But in our study, as mentioned before, only the aiding flow is considered. The final steady-state flow and heat transfer characteristics will be presented in the subsequent sections.

2.1 Boundary Conditions

It is mentioned before that the temperature of the isothermal walls , T_w is assumed to be 1K. The temperature of the flow passing through the inlet, T_0, is considered to be 0K above the freezing point of water. So, the boundary conditions of Eqs. (11) and (12) are

Boundary Condition for all walls being isothermal-

Left isothermal wall: $\psi = 0, \quad T = T_w = 1$ on $x = 0, \quad 0 \le y \le H, \quad \ldots 14(i)$

Inlet: $\psi = -xV_0, \quad T = T_0 = 0$ on $y = 0, \quad 0 \le x \le I \ldots 14(ii)$

Bottom Isothermal wall: $\psi = 0, \quad T = T_w = 1$ on $y = 0, \quad I \le x \le W \ldots 14(iii)$

Right Isothermal wall: $\psi = 0, \quad T = T_w = 1$ on $x = W, \quad 0 \le y \le H \ldots 4(iv)$

Top Isothermal wall: $\psi = 0, \quad T = T_w = 1$ on $y = H, \quad O \le x \le W, \ldots 14(v)$

Outlet: $\frac{\partial\psi}{\partial y} = 0, \quad \frac{\partial T}{\partial y} = 0$ on $y = H, 0 \le x \le O \quad \ldots \ldots 14(vi)$

Boundary Condition for left wall isothermal & remaining walls being adiabatic-

Left isothermal wall: $\psi = 0, \quad T = T_w = 1$ on $x = 0, \quad 0 \le y \le H, \quad \ldots 15(i)$

Inlet: $\psi = -xV_0, \quad T = T_0 = 0$ on $y = 0, \quad 0 \le x \le I, \quad \ldots \quad 15(ii)$

Bottom Adiabatic wall: $\psi = -I \times V_0, \quad \frac{\partial T}{\partial y} = 0$ on $y = 0, \quad I \le x \le W, \quad \ldots \quad 15(iii)$

Right Adiabatic wall: $\psi = -I \times V_0, \quad \frac{\partial T}{\partial x} = 0$ on $x = W, \quad 0 \le y \le H, \quad \ldots \quad 15(iv)$

Top Adiabatic wall: $\psi = -I \times V_0$, $\frac{\partial T}{\partial y} = 0$ on $y = H$, $O \le x \le W$, ... 15(v)

Outlet: $\frac{\partial \psi}{\partial y} = 0$, $\frac{\partial T}{\partial y} = 0$ on $y = H$, $0 \le x \le O$ ... 15(vi)

It should be noticed that the vertical velocity component, v, is numerically equal to V_0 at the inlet. Hence the stream-function value at the inlet can be obtained by integrating v from Eq. (10) with respect to x between the limits 0 and I/W. This gives the boundary condition (14(ii)) for ψ. The other three Isothermal surfaces of the cavity are connected together, and hence they all have the same constant value of $\psi = -I \times V_0$. For the inlet flow, the temperature is known and it is set numerically equal to zero.

The assumption of outlet boundary condition is not easy. Convection is assumed to be dominant in the outflow through the vent. The conduction through the outlet will then be almost negligible. Hence the temperature gradient ($\frac{\partial T}{\partial y} = 0$) is assumed to be zero at the outlet. Several authors used such a boundary condition for the energy equation at the outlet boundary; for example, Prasad et al. [19] for porous media and Angirasa [20] for non-porous media. It is seen that Eqs. (11) and (12) subject to the boundary conditions (14 and 15) involve three parameters, namely, *Ra, Pe*, and *I/W*. The relative magnitude of the Rayleigh and Pe´clet numbers determine which of the two mechanisms of forced or free convection flow is predominant.

2.2 Physical Quantities of Interest

The physical quantities of interest in this problem are the local Nusselt number, Local Entropy generation number, Bejan Number and Energy Flux Density.

The local Nusselt Number along the isothermal wall is defined by

$$\mathrm{Nu}_{x=0} = -\frac{H}{\Delta T}\left(\frac{\partial T}{\partial x}\right) \quad \ldots \quad \ldots \quad \ldots \quad \ldots \quad \ldots \quad \ldots \quad (16)$$

and the average Nusselt number along the hot wall is defined as

$$Nu_{av} = \frac{\int_0^H |Nu_{x=0}| dy}{\int_0^H dy} \quad \ldots \quad \ldots \quad \ldots \quad \ldots \quad \ldots \quad \ldots \quad (17)$$

The local Entropy Generation Number is defined by

$$Ns = \frac{S'''_{gen}}{S'''_0} = \left[\left(\frac{\partial T}{\partial x}\right)^2 + \left(\frac{\partial T}{\partial y}\right)^2\right] + \frac{Ec \times \Pr}{\frac{\Delta T}{T_0}}\left[\left(\frac{\partial \psi}{\partial x}\right)^2 + \left(\frac{\partial \psi}{\partial y}\right)^2\right] = Ns_\tau + Ns_F \quad \cdots \quad (18)$$

The definitions of different parameters in Eq. (12) to Eq. (13) are as follows:

$$S'''_0 = \frac{k(\Delta T)^2}{H^2 T_0^2}, \qquad Ec = \left(\frac{\alpha_m}{H}\right)^2 \frac{C_P}{\Delta T} \quad \ldots \quad \ldots \quad \ldots \quad (19)$$

and the average Nusselt number is defined as

$$Ns_{av} = \frac{\int_0^W \int_0^H Ns\,dy\,dx}{\int_0^W \int_0^H dy\,dx} \quad \ldots \quad \ldots \quad \ldots \quad \ldots \quad (20)$$

The local Bejan Number is defined by

$$Be = \frac{HTI}{S'''_{gen}} \quad \ldots \quad \ldots \quad \ldots \quad \ldots \quad \ldots \quad \ldots \quad (21)$$

and the average Bejan Number is defined as

$$Be_{av} = ST_{av} + SF_{av} \quad \ldots \quad \ldots \quad \ldots \quad \ldots \quad \ldots \quad \ldots \quad (22)$$

where

$$ST_{av} = \frac{\int_0^W \int_0^H HTI\,dy\,dx}{\int_0^W \int_0^H dy\,dx} \quad \text{and} \quad SF_{av} = \frac{\int_0^W \int_0^H FFI\,dy\,dx}{\int_0^W \int_0^H dy\,dx} \quad \ldots \quad \ldots \quad (23)$$

From Eq. (3.8) we can obtain the x and y components of energy flux density. They are

$$E_x = \rho_0 u\left(\frac{u^2 + v^2}{2} + C_P T\right) - k\frac{\partial T}{\partial x} \quad \ldots \quad \ldots \quad \ldots \quad \ldots \quad (25)$$

and

$$E_y = \rho_0 v\left(\frac{u^2 + v^2}{2} + C_P T\right) - k\frac{\partial T}{\partial y} \quad \ldots \quad \ldots \quad \ldots \quad (26)$$

So, local energy flux density is

$$E = \sqrt{E_x^2 + E_y^2} \quad \ldots \quad \ldots \quad \ldots \quad \ldots \quad \ldots \quad (27)$$

Similarly the average energy flux density is

$$E_{av} = \frac{\int_0^W \int_0^H E dy dx}{\int_0^W \int_0^H dy dx} \quad \ldots \quad \ldots \quad \ldots \quad \ldots \quad \ldots \quad (28)$$

The unstructured grid system, as shown in Fig.2, is used for the present computations. All the above mentioned equations, accompanied with their boundary conditions, are discretized by a finite element formulation. The numerical solution procedure adopts the well known semi-implicit SIMPLE algorithm. The convergence criteria are set as the relative residual of all variables, including mass, all velocity components and temperature, less than 10^{-5}. Validated CFD software is used for the numerical solutions.

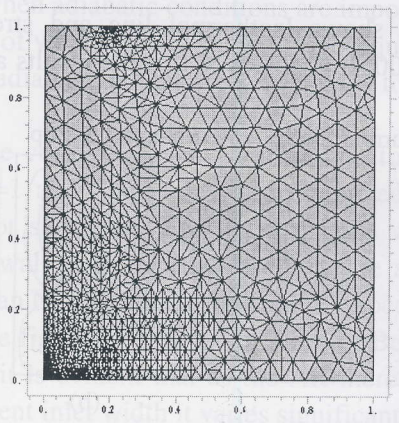

Figure 2: Generated mesh for analysis

3 VALIDATION

For validity results of this study is compared with Mahmud and Pop [17]. The data are taken from the Table 4 of that paper which represents the value of Average Nusselt Number for adiabatic aiding flow situation where the aspect ratio is 1, inlet width to cavity width ratio is 0.25 and the inlet width to outlet width ratio is 1. From the Fig.3 it appears that the numerical analysis done in our study produces such results which is almost equal to the results of Mahmud and Pop.

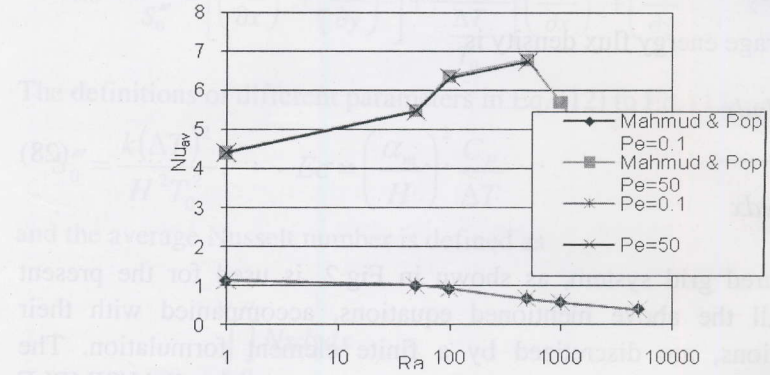

Figure 3: Variation Nu_{av} with Ra for different Pe/clet Numbers(Adiabatic Aiding Flow, AR=1, I/W=0.25, I/O=1)

The next figure (Fig.4) shows Isothermal line and stream lines for AR=,1 I/W=0.25, Pe=0.1, Ra=100. It is observed that the results are almost similar as it is done in this study.

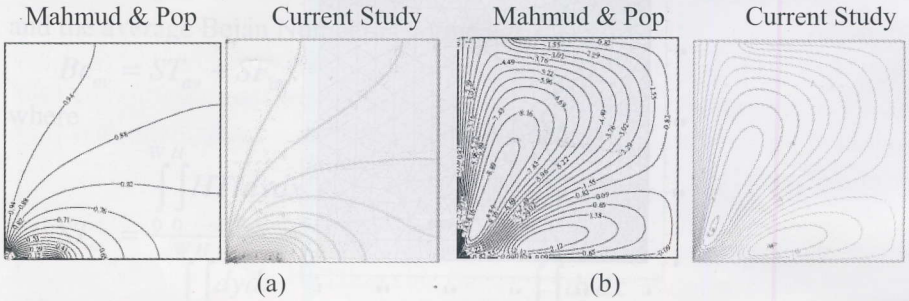

Figure 4: (a) Isothermal lines (b) Streamlines for AR=1, I/W=0.25, Pe=0.1, Ra=100

4 RESULTS AND DISCUSSION

When all the walls are isothermal; Fig.5 (a) shows the isothermal lines for different Aspect Ratio, I/W=0.25, I/O=0.5 Ra=1 and Pe=0.1. The variation of isothermal lines with the change of aspect ratio is observed. It is evident from the figure that initially the isothermal lines are well spread towards right wall but gets confined near the left isothermal wall as aspect ratio (AR=2) increases. Thus it can be concluded that the rate of change of temperature increases with increasing of aspect ratio & decreases with decreasing of aspect ratio. Again the

isothermal lines cover less area of the porous media as aspect ratio increases. Fig.5 (b) demonstrates the isothermal lines when adiabatic boundary conditions are applied. It is apparent from the figure that near the isothermal wall the isothermal lines are denser as the aspect ratio reduces and the spread of isothermal lines increases with the increase of aspect ratio. Thus it can be concluded that the rate of change of temperature decreases with the increase of aspect ratio. Again the isothermal lines cover more area of the porous media with the increase of aspect ratio.

Fig.6 (a) shows the streamlines for I/W=0.4, I/O=0.5, Ra=1 and Pe=0.1. The variation of streamline with the change of aspect ratio is observed when the walls are isothermal. As the aspect ratio increases, consequently density of streamlines at the right isothermal wall increases. At low aspect ratio, the fluid flow continues with formation of vortices .The vortex size decreases as the aspect ratio increase and thus facilitates heat transfer & recovering of lost energy.

As depicted in Fig.6 (b), streamlines follows almost similar trend to isothermal condition when adiabatic conditions are imposed .The only noticeable difference is the delay of vortex formation & its subsequent increase of size with increase of AR due to adiabatic boundaries compared to that with all isothermal walls.

Observation on the constant Bejan Number line for different aspect ratio, I/W=0.5,I/O=0.5 , Ra=1 and Pe=0.1 has been depicted in Fig. 7(a). Constant Bejan number does not show any significant change with variation of aspect ratio. When only left wall is isothermal & others are adiabatic then Fig.7 (b) shows the constant Bejan Number line for different aspect ratio, I/W=0.5, I/O=1, Ra=1 and Pe=0.1.These figures show the variation of Bejan number with aspect ratio. From the figure it is evident that as the AR increases, the Bejan contour increases and for different inlet width it varies significantly.

On the other hand , for different aspect ratio, I/O=0.5, different Rayleigh number and Peclet number, Average Entropy Generation Number Ns_{av} increases with the increase of Aspect Ratio & moves towards a steady value. From Fig.8 (a) it is observed that the value of Ns_{av} increases by 210% , 243.2% 200.6% ,212.28%, 141.936% ,74.6% , 58.55% for Pe= 0.1, 1, 5, 10, 20, 50, 100 respectively when aspect ratio increases from 0.5 to 2 for I/W=0.1, I/O=0.5, Ra=100.

Fig.8 (b) shows the variation of Average Entropy Generation Number with Aspect Ratio for different Rayleigh number & Peclet number. It is evident from these figures that Ns_{av} increases with the increase of Aspect Ratio. From Fig.8 (b) it is observed that the value of Ns_{av} increases by 159.8%, 156%,

137.6%, 109.9%, 67.5%, 39.67, 76.38% for Pe= 0.1, 1, 5, 10, 20, 50, 100 respectively when AR increases from 0.5 to 1.5 for I/W=0.1, I/O=0.5, Ra=100.

From the Fig.8 it is evident that for high Pe, the Ns_{av} is higher and for low Pe, Ns_{av} is lower. It is found from this study that value of the Ns_{av} is the maximum where Ra and Pe both are the maximum and it has the minimum value when Pe is the minimum but Ra is the maximum. From these observations we can comment that for the situations where forced convection is dominating the rate of entropy generation is high but for mixed convection situations the rate of entropy generation is lower.

Fig.9 (a) shows the variation of Average Nusselt Number with Aspect Ratio for different Pe. It is evident from these figures that for low Peclet numbers Nu_{av} increases with the increase of Aspect Ratio. From Fig.9 (a), it is observed that for Peclet number (0.1, 1) the value of Nu_{av} increases by 31.4%, 24.5%. But as Peclet number increases Nu_{av} decreases with increasing AR. For Pe=10, 20, 50, 100 Nu_{av} decreases by 10.8%, 3.8%, 4.8%, 7.18%, 7.53% when aspect ratio increases from 0.5 to 2 for I/W=0.1, I/O=0.5, Ra=100.

Fig.9 (b) shows the variation of Average Nusselt Number with Aspect Ratio for different Pe. It is evident from this figure that Nu_{av} decreases with the increase of Aspect Ratio. From Fig.9 (b) it is observed that the value of Nu_{av} increases by 6.12%, 1.2% for Pe= 0.1, 1 and then follows a decrease of 15.9%, 30.62%, 47.03%, 57.4%, 42.3% for Pe= 5, 10, 20, 50, 100 respectively when AR increases from 0.5 to 1.5 for I/W=0.1, I/O=0.5, Ra=100. It is also evident that the rate of change of Nu_{av} is higher for higher Ra. At AR=0.5, I/W=0.1, I/O=0.5, Ra=50, Pe=100 for all walls Isothermal the value of Ns_{av} is 81.21707 but for left wall adiabatic and rest walls isothermal Ns_{av} is 84.47173

From Fig.9 it is also evident that as the Peclet Number increases the value of average Nusselt Number increases. From this analysis it is also clear that for high Peclet Numbers, Nu_{av} increases with the increase of the value of Ra and for low Peclet Number Nu_{av} decreases with the increasing of Ra. For a particular Pe, Nu_{av} is the highest for mixed convection situation. Table 1 shows the numerical values of Average Nusselt Number for different Aspect Ratio and at different boundary conditions for Pe=10, I/W=0.1 and I/O=0.5.

Fig.10 (a) shows the variation of Average Bejan Number with aspect ratio for different Pe. It is evident from this figure that Be_{av} increases with the increase of aspect ratio. It is observed from Fig.10 (a) that the value of Be_{av} increases by 4.03%, 3.75%, 7.4%, 15.58 %, 33.16%, 42.82%, 20.46% for Pe= 0.1, 1, 5, 10, 20, 50, 100 respectively when aspect ratio increases from 0.5 to 2 for I/W=0.1, I/O=0.5, Ra=50.

Table 1: Values of Average Nusselt Number for different Aspect Ratio and at different boundary conditions for Pe=10, I/W=0.1 and I/O=0.5

	All walls are isothermal			Left wall is Isothermal, remaining walls are adiabatic		
	AR=0.5	AR=1	AR=2	AR=0.5	AR=1	AR=1.5
Ra=1	2.367834	1.215259	0.608591	2.960986	2.494	2.024954
Ra=50	2.104044	1.046838	0.554921	3.891656	2.632	1.969932
Ra=100	1.80619	0.90626	0.508465	4.412873	2.58	1.875746
Ra=500	0.724795	0.412423	0.296742	3.641727	1.802	1.324122

Fig.10 (b) shows the variation of Average Bejan Number with Aspect Ratio for different Pe. It is evident from this figure that Be_{av} increases with the increasing of Aspect Ratio. It is observed from Fig.10 (b) that the value of Be_{av} increases by 6.8%, 8%, 15%, 25.4%, 36.22%, 31.8%, 22.56% for Pe= 0.1, 1, 5, 10, 20, 50, 100 respectively when AR increases from 0.5 to 1.5 for I/W=0.1, I/O=0.5, Ra=50. At AR=0.5, I/W=0.1, I/O=0.5, Ra=50, Pe=100 for all walls Isothermal the value of Be_{av} 0.055352 but for left wall adiabatic and rest walls isothermal Be_{av}=0.036948.

From Fig.10 it is evident that as the value of Pe increases Be_{av} decreases. It is found from this analysis that Be_{av} is the lowest for low Ra and high Pe and Be_{av} is the highest for low Pe and low Ra.

Fig.11 (a) demonstrates variation of Average Energy Flux Density with Aspect Ratio for different Pe. E_{av} decreases significantly with the increase of aspect ratio. The decrease rate is higher at low aspect ratio but slows down at high AR. Referring to Fig.11 (a), value of E_{av} decreases by 72.3%, 71.3% ,66.6%, 64.7%, 66.7%, 78.9%, 89.16% for Pe= 0.1, 1, 5, 10, 20, 50 and 100 respectively when aspect ratio increases from 0.5 to 2 for I/W=0.1, I/O=0.5, Ra=100.

Fig.11 (b) shows the variation of Average Energy Flux Density with Aspect Ratio for different Pe. It is evident from these figures that E_{av} decreases with the increase of Aspect Ratio. It is observed from Fig.11 (b) that the value of E_{av} decreases by 44.7%, 45.8%, 49.7%, 53.3%, 60.775%, 79.003% for Pe= 0.1, 1, 5, 10, 20, 50 and 100 respectively when AR increases from 0.5 to 1.5 for I/W=0.1, I/O=0.5, Ra=100. At AR=0.5, I/W=0.1, I/O=0.5, Ra=100, Pe=100 for all walls Isothermal the value of E_{av} is1.859998 but for left wall adiabatic and rest walls isothermal E_{av} is 2.149177.

Fig.11 also shows that Average Energy Flux Density (E_{av}) increases with the increase of Pe. In this study it is also observed that E_{av} decreases with the decreasing of Ra.

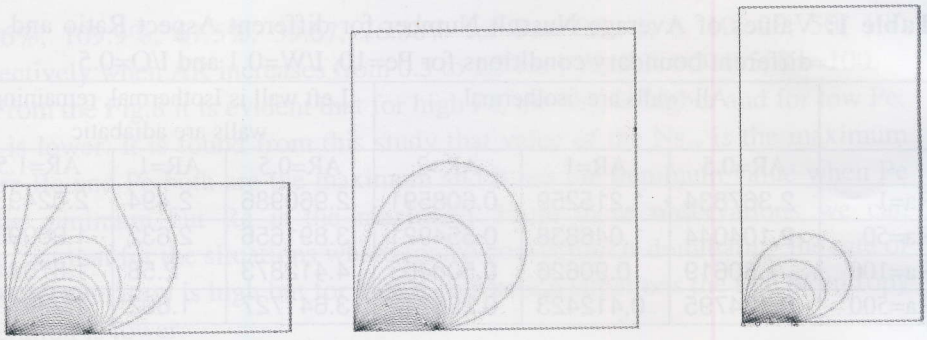

AR=0.5 AR=1 AR=2

(a)Wall condition: All walls are isothermal

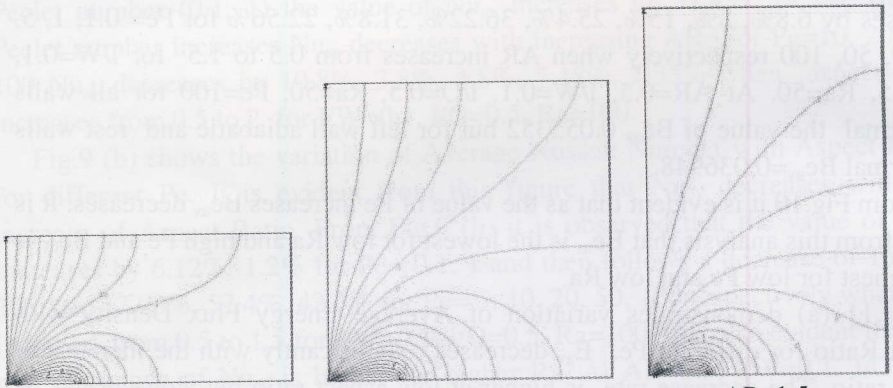

AR=0.5 AR=1 AR=1.5

(b)Wall condition: Left wall is Isothermal, remaining walls are adiabatic

Figure 5: Isothermal Line for I/W=0.25, I/O=0.5, Ra=1 and Pe=0.1

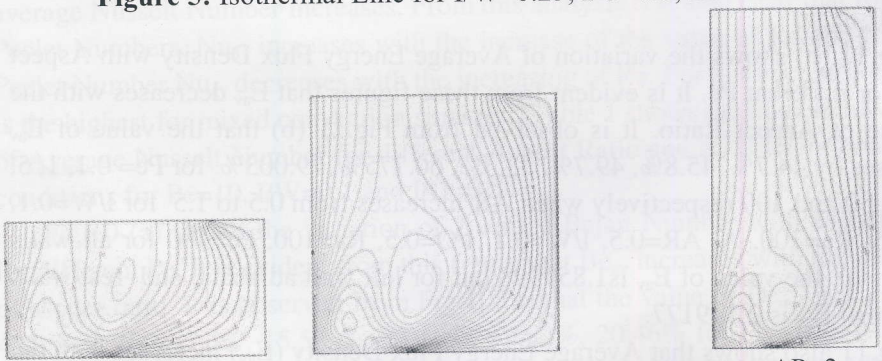

AR=0.5 AR=1 AR=2

(a) Wall condition: All walls are isothermal

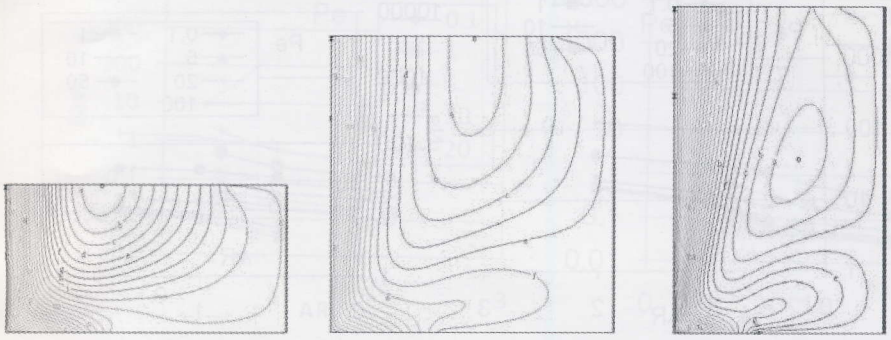

AR=0.5 AR=1 AR=1.5

(b) Wall condition: Left wall is Isothermal, remaining walls are adiabatic

Figure 6: Streamline for I/W=0.4, I/O=0.5, Ra=1 and Pe=0.1

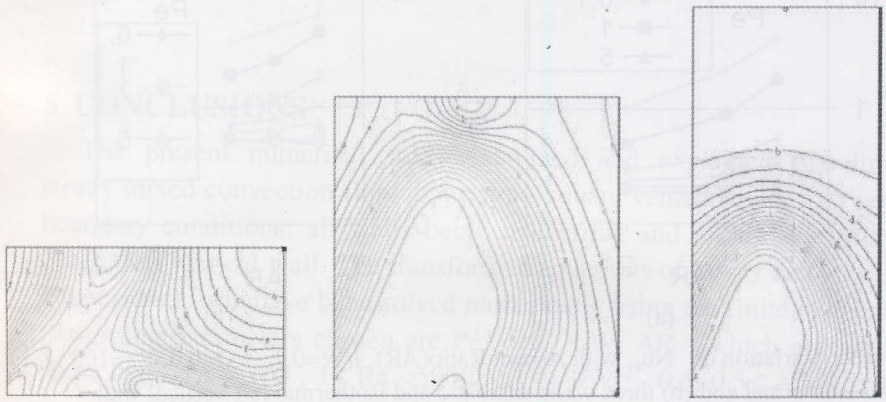

AR=0.5 AR=1 AR=2

(a)Wall condition: All walls are isothermal

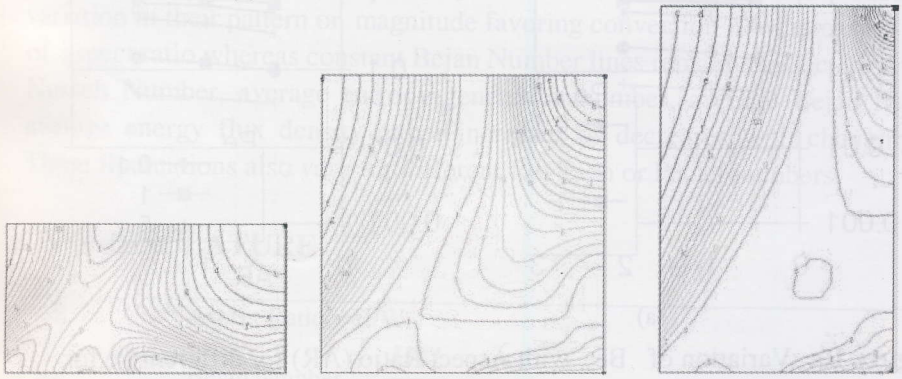

AR=0.5 AR=1 AR=1.5

(b)Wall condition: Left wall is Isothermal, remaining walls are adiabatic

Figure 7: Constant Bejan Number line for I/W=0.5, I/O=0.5, Ra=1 and Pe=0.1

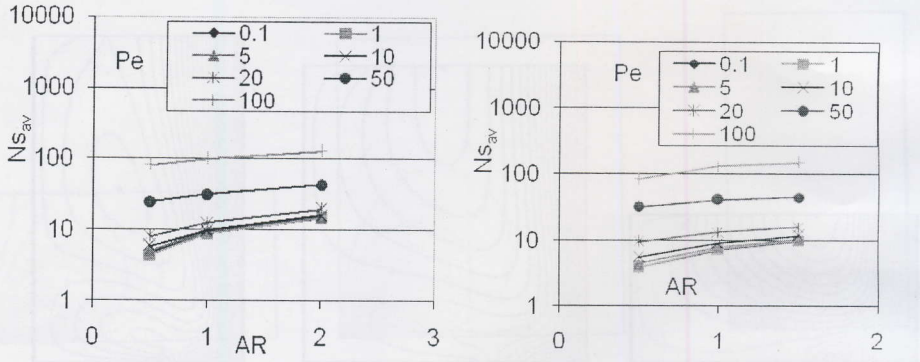

Figure 8: Variation of Ns_{av} with Aspect Ratio(AR) I/W=0.1, I/O=0.5, Ra=100 for (a) all wall isothermal and (b) three walls adiabatic and isothermal left vertical wall

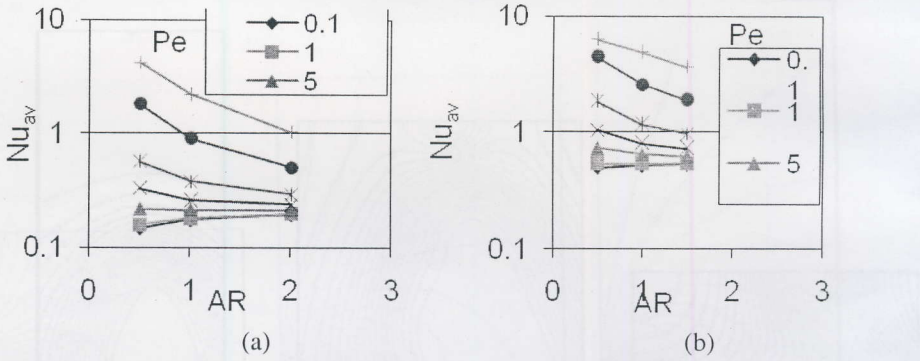

Figure 9: Variation of Nu_{av} with Aspect Ratio(AR) I/W=0.1, I/O=0.5, Ra=100 for (a) all wall isothermal and (b) three walls adiabatic and isothermal left vertical wall.

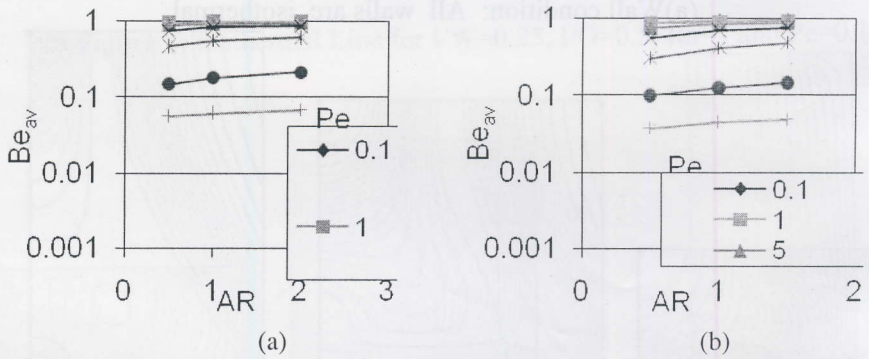

Figure 10: Variation of Be_{av} with Aspect Ratio (AR) for different Pe for I/W=0.1, I/O=0.5 ,Ra=50 for (a) all wall isothermal and (b) three walls adiabatic and isothermal left vertical wall.

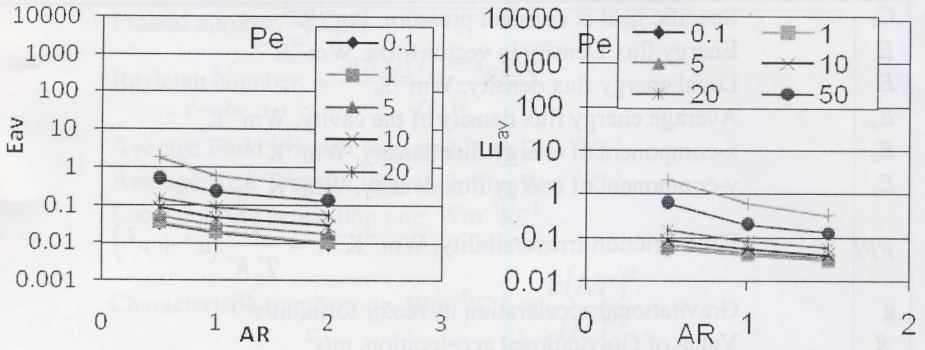

Figure 11: Variation of E_{av} with Aspect Ratio (AR) for different Pe for I/W=0.1, I/O=0.5,Ra=100 for (a) all wall isothermal and (b) three walls adiabatic and isothermal left vertical wall.

5 CONCLUSIONS

The present numerical study examined and explained two-dimensional, steady mixed convection flow in a porous square vented cavity for two different boundary conditions; all walls being isothermal and all walls being adiabatic except left vertical wall. The transformed equations of Darcy and energy in non-dimensional form have been solved numerically using the finite element method. Governing parameters chosen are Pe , Ra, I/W, AR which are varied in the range $0.1 \leq Pe \leq 100$, $1< Ra <5000$, $0.1\leq$ I/W $\leq$ 0.5, $0.5\leq AR \leq 2$ .It is clear from the results that aspect ratio has considerable influence on the flow and heat transfer characteristics in the cavity. Isotherms, streamlines show substantial variation in their pattern or magnitude favoring convection for increasing values of aspect ratio whereas constant Bejan Number lines remain unaffected. Average Nusselt Number, average entropy generation number, average Bejan Number, average energy flux density either increases or decreases with changing AR. These fluctuations also vary for different Rayleigh or Peclet numbers.

6 NOMENCLATURE

AR	Aspect Ratio, =H/W
Be	Bejan Number, $= \dfrac{HTI}{S'''_{gen}}$
Be_{av}	Average Bejan Number

C_P	Specific heat at constant pressure, $Jkg^{-1}K^{-1}$
$\boldsymbol{E}$	Energy flux Density in vector form, $Wm^{-3}K^{-1}$
E	Local energy flux density, $Wm^{-3}K^{-1}$
E_{av}	Average energy flux density of the cavity, $Wm^{-3}K^{-1}$
E_x	x-component of energy flux density, $Wm^{-3}K^{-1}$
E_y	y-component of energy flux density, $Wm^{-3}K^{-1}$
FFI	Fluid Friction Irreversibility, $Wm^{-3}K^{-1}$, $=\frac{\mu}{T_0 K}\left(u^2+v^2\right)$
$\mathbf{g}$	Gravitational acceleration in vector form, m/s^2
g	Value of Gravitational acceleration, m/s^2
H	Cavity height, m
HTI	Heat Transfer Irreversibility, $Wm^{-3}K^{-1}$, $=\frac{k}{T_0^2}\left[\left(\frac{\partial T}{\partial x}\right)^2+\left(\frac{\partial T}{\partial y}\right)^2\right]$
I	Width of the inlet, m
$\boldsymbol{i}$	Unit vector in x-direction
$\boldsymbol{j}$	Unit vector in y-direction
K	permeability of the porous medium, m^2
k	Thermal conductivity of the fluid, $Wm^{-1}K^{-1}$
$\boldsymbol{k}$	Unit vector in z-direction
Nu	Local Nusselt Number
$Nu_{x=0}$	Local Nusselt Number at the Isothermal Wall, $=-\frac{H}{\Delta T}\left(\frac{\partial T}{\partial x}\right)_{x=0}$
Nu_{av}	Average Nusselt number of the Isothermal Wall, $=\frac{\int_0^H \lvert Nu_{x=0}\rvert dy}{\int_0^H dy}$
Ns	Local Entropy Generation Number, $=\frac{S'''_{gen}}{S'''_0}$
Ns_{av}	Average Entropy Generation Number
O	Width of the vent, m
p	Pressure, Pa
Pe	Pe´clet number, $=\frac{V_0 H}{\alpha_m}$

Pr	Prandtl number, $=\mu Cp/k$
Ra	Rayleigh Number, $= \frac{gK\beta(T_w - T_0)H}{\alpha_m \nu}$
SF_{av}	Average Fluid Friction Irreversibility, $Wm^{-3}K^{-1}$
ST_{av}	Average Heat Transfer Irreversibility, $Wm^{-3}K^{-1}$
S'''_{gen}	Local entropy generation rate, $Wm^{-3}K^{-1}$
S'''_0	Characteristic transfer rate, $Wm^{-3}K^{-1}, = \frac{k(\Delta T)^2}{H^2 T_0^2}$
t	Time, s
T	Fluid Temperature, ^oC
T_0	Temperature of the through flow at the inlet, ^oC
Tw	Temperature of the isothermal vertical wall, ^oC
ΔT	Temperature Difference between flow at the inlet and isothermal wall, ^oC, $=T_w-T_0$
u	velocity components along y-axis, m s^{-1}
v	velocity components along y-axis, m s^{-1}
v	velocity vector, m s^{-1}
V	Volume of the sample, m^3
V_0	Absolute value of the velocity of the forced flow at the inlet, ms^{-1}
W	Width of the cavity, m
x	Cartesian coordinates, m
y	Cartesian coordinates, m
Greek Symbols	
α_m	Effective thermal diffusivity, $m^2\ s^{-1}$
β	coefficient of thermal expansion, K^{-1}
σ	Ratio of composite material heat capacity to convective fluid heat capacity
ϕ	Porosity of the porous medium
ρ	Density of the fluid, Kg/m^3
μ	Dynamic viscosity of the fluid, Pa□s
ν	kinematic viscosity, m^2s^{-1}
(ψ)	volume-averaged quantity, $= \frac{1}{V}\iiint_v \psi\, dV$
ψ	Stream Function

7 REFERENCES

[1] D.A. Nield, A. Bejan, Convection in Porous Media, second ed.,Springer, New York, 1999.

[2] D.B. Ingham, I. Pop (Eds.), Transport Phenomena in Porous Media, Pergamon, Oxford, 1998.

[3] D.B. Ingham, I. Pop (Eds.), Transport Phenomena in Porous Media, Pergamon, Oxford, 2002.

[4] D.B. Ingham, I. Pop (Eds.), Transport Phenomena in Porous Media, Elsevier, Oxford, 2005.

[5] K. Vafai (Ed.), Handbook of Porous Media, Marcel Dekker, NewYork, 2000.

[6] K. Vafai (Ed.), Handbook of Porous Media, second ed., Taylor & Francis, New York, 2005.

[7] I. Pop, D.B. Ingham, Convective Heat Transfer: Mathematical and Computational Modeling of Viscous FluidPorous Media,Pergamon, Oxford, 2001.

[8] A. Bejan, A.D. Kraus (Eds.), Heat Transfer Handbook, Wiley, New York, 2003.

[9] D.B. Ingham, A. Bejan, E. Mamut, I. Pop (Eds.), Emerging Technologies and Techniques in Porous Media,Kluwer, Dordrecht,2004.

[10] A. Bejan, I. Dincer, S. Lorente, A.F. Miguel, A.H. Reis, Porous and Complex Flow Structures in Modern Technologies, Springer, NewYork, 2004.

[11] H. Hadim, K. Vafai, Overview of current computational studies ofheat transfer in porous media and their applications—forcedconvection and multiphase heat transfer, in: W.J. Minkowycz, E.M.Sparrow (Eds.), Advances in Numerical Heat Transfer, vol. II, Taylorand Francis, New York, 2000, pp. 291–329.

[12] K. Vafai, H. Hadim, Overview of current computational studies ofheat transfer in porous media and
their applications—natural andmixed convection, in: W.J. Minkowycz, E.M. Sparrow (Eds.),Advances in Numerical Heat Transfer, vol. II, Taylor and Francis,New York, 2000, pp. 331–369.

[13] O. Kvernvold and P. A. Tyvand, 1979, "Nonlinear thermal convection in anisotropic porous media", Journal of Fluid Mechanics Digital Archive, vol. 90, p. 609-624, Cambridge University Press

[14] K. Vafai, 1984, "Convective flow and heat transfer in variable-porosity media", Journal of Fluid Mechanics Digital Archive (1984), vol. 147, pp. 233-259, Cambridge University Press

[15] A. Younes, "An accurate moving grid Eulerian Lagrangian localized adjoint method for solving the one-dimensional variable-coefficient", International Journal for Numerical Methods in Fluids, vol. 45, no. 2, pp. 157-178.

[16] J. C. F. Wong and P. Yuan, "Mixed finite element formulation of algorithms for double-diffusive convection in a fluid-saturated porous medium", Communications in Numerical Methods in Engineering, Published online in Wiley InterScience (www.interscience.wiley.com).

[17] S. Mahmud and I. Pop, 2006, "Mixed convection in a square vented enclosure filled with a porous medium", International Journal of Heat and Mass Transfer vol. 49 (2006), pp. 2190–2206

[18] S. Mahmud, R.A. Fraser, Magnetohydrodynamic free convectionand entropy generation in a square porous cavity Int J. Heat MassTransfer 47 (2004) 3245–3256.

[19] D. Angirasa, Mixed convection in a vented enclosure with anisothermal vertical surface, Fluid Dyn. Res. 26 (2000) 219–233.

[20] V. Prasad, F.C. Lai, F.A. Kulacki, Mixed convection in horizontalporous layers heated from below, J. Heat Transfer 110 (1988) 395-402.